JPL Publication 04-008

Scientific Impacts of Wind Direction Errors

W. Timothy Liu, Seung-Bum Kim, Tong Lee, Y. Tony Song, and Wenqing Tang
Jet Propulsion Laboratory, Pasadena, California

Robert Atlas
Goddard Space Flight Center, Greenbelt, Maryland

National Aeronautics and
Space Administration

Jet Propulsion Laboratory
California Institute of Technology
Pasadena, California

May 2004

The research described in this publication was carried out at the Jet Propulsion Laboratory, California Institute of Technology, under contract with the National Aeronautics and Space Administration (NASA). It was supported by NASA's Ocean Vector Wind Program. A portion of the work was performed at the NASA Goddard Space Flight Center, Greenbelt, Maryland.

ABSTRACT

An assessment on the scientific impact of random errors in wind direction (< 45°) retrieved from space-based observations under weak wind (< 7 m/s) conditions was made. Half of the winds over global oceans are below 7 m/s, in their long-term averages, and these weak winds cover most of the tropical, sub-tropical, and coastal oceans. Introduction of these errors in the semi-daily winds causes, on average, 5% changes of the yearly mean Ekman and Sverdrup volume transports computed directly from the winds, respectively. These poleward movements of water are the main mechanisms to redistribute heat from the warmer tropical region to the colder high-latitude regions, and they are the major manifestations of the ocean's function in modifying Earth's climate. Simulation by an ocean general circulation model shows that the wind errors introduce a 5% error in the meridional heat transport at tropical latitudes. The simulation also shows that the erroneous winds cause a pile-up of warm surface water in the eastern tropical Pacific, similar to the conditions during El Niño episode. Similar wind directional errors cause significant change in sea-surface temperature and sea-level patterns in coastal oceans in a coastal model simulation. Previous studies have shown that assimilation of scatterometer winds improves 3–5 day weather forecasts in the Southern Hemisphere. When directional information below 7 m/s was withheld, approximately 40% of the improvement was lost.

ACKNOWLEDGMENTS

Yunjin Kim and Victor Zlotnicki of Jet Propulsion Laboratory first articulated the need of this study.

TABLE OF CONTENTS

Section 1. Introduction

Even for the proven technique of scatterometry, the accuracy of retrieving vector winds is degraded below a wind-speed threshold of about 2–3 m/s (e.g., Freilich, 1999; Plant, 2000). The threshold appears to be much higher for the experimental technique of polarimetric radiometry. The United States Windsat/Coriolis mission, launched in January 2003, was the first instrument designed to demonstrate the polarimetric radiometer approach for acquiring accurate, all-weather measurements of surface vector winds from space. It will serve as a risk reduction program for the Conical Microwave Imager Sounder (CMIS) to operate on the National Polar-orbiting Operational Environmental Satellite System (NPOESS). The prelaunch aircraft flight experiments demonstrated appreciable wind direction signals for moderate and high winds (> 7 m/s), but also indicated insufficient sensitivity to wind direction for lighter winds (below 7 m/s) at Windsat incident angles (e.g., Yueh et al., 1999).

This is a report on the potential scientific impacts caused by anticipated errors in wind direction. To understand the amount and location of winds under the threshold, the distribution of the mean and variability of winds over global ocean computed by Wenqing Tang is described in Section 2. The wind data used in the ocean studies are described in Section 3.1.

Ocean affects climate mainly by storing solar heating during the warmer seasons and releasing it in colder seasons and by moving the heat from the warm ocean in low latitudes to the cooler oceans in high latitudes. Zonal redistribution of heat in the ocean mixed layer, caused by the relaxation of the trade winds in the equatorial Pacific, also causes the major climate episodes of El Niño and La Niña. The meridional redistribution of heat is accomplished through wind-driven Ekman and Sverdrup transport, the impact of which, as computed by Seung-Bum Kim, is described in Section 3.2. Through an ocean general circulation model (OGCM), Tong Lee simulated the sea surface temperature and surface dynamic topography and the impact on meridional heat transport and zonal heat distribution in the tropical ocean; his results are presented in Section 3.3. Large portions of the population lives near the coast, and coastal oceans are the most productive parts of the global oceans. Coastal oceans are known to be more sensitive to surface forcing than open oceans because the momentum and energy from the atmosphere are absorbed by relatively small volumes of shallow water. The impact of a coastal ocean simulated by a coastal model by Tony Song is described in Section 4. Weather affects our daily lives and the impact in global numerical weather prediction by Robert Atlas is explained in Section 5.

Section 2. Distribution of Winds Under Threshold

Figure 1, based on 4 years of daily-gridded ocean wind vector measurements from September 1999 to August 2003, is derived from the NASA's QuikSCAT scatterometer and shows that half of winds blowing over the global ocean are under 7 m/s, and a fourth are under 5 m/s. In general, the wind speeds derived from Special Sensor Microwave Imager may have slightly higher values and those from the scatterometers on European remote sensing satellites may have slightly lower values than QuikSCAT measurements, while the numerical weather prediction (NWP) products of the National Center for Environmental Prediction (NCEP) have good agreement with QuikSCAT measurements. It is clear from Figure 2 that the average wind speeds are below 5 m/s for most of the tropical and coastal oceans. The subtropical oceans will also be included if the threshold is moved up to 7 m/s.

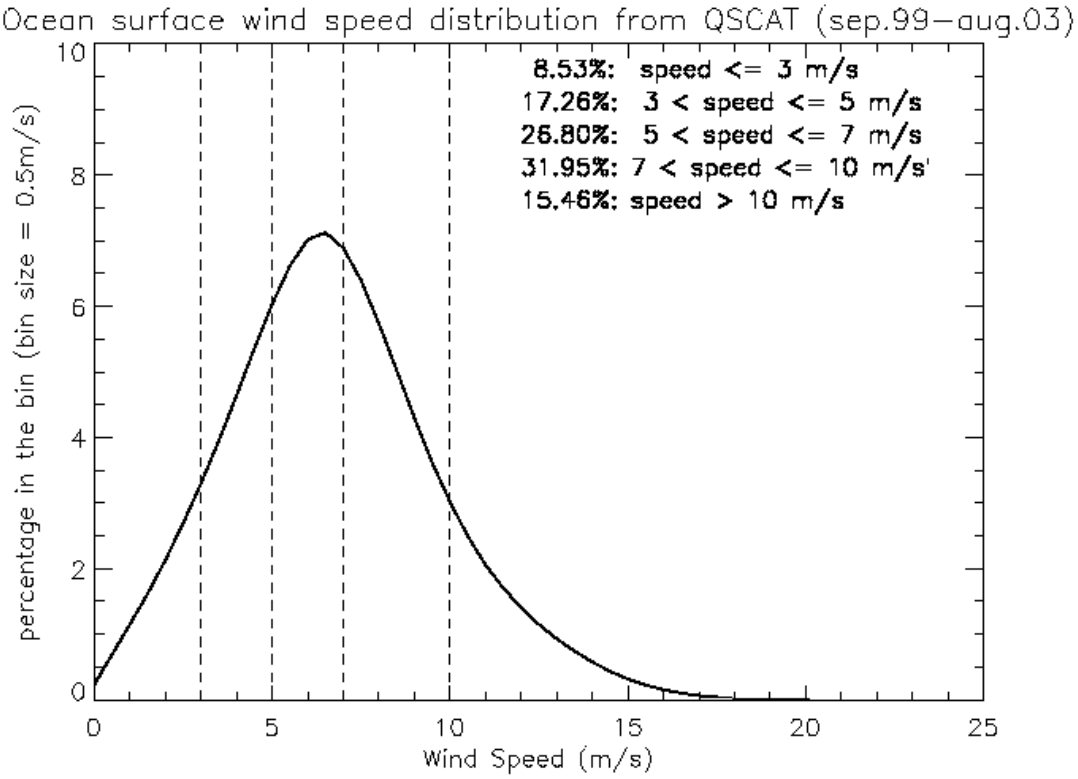

Figure 1. Percentage wind distribution derived from four years (September 1999 – August 2003) of measurements by QuikSCAT. The cumulative percentage of winds falling within certain ranges are also shown.

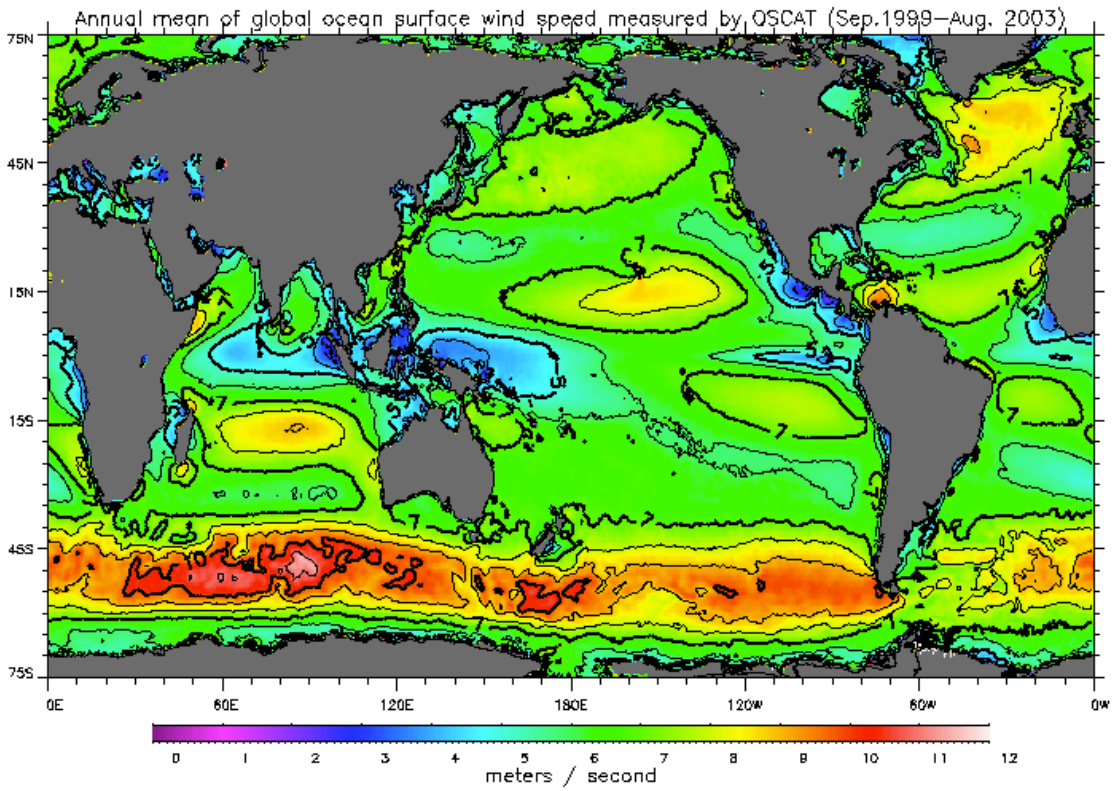

Figure 2. Averaged wind speed derived from four years (September 1999 to August 2003) of QuikSCAT data. Isotach interval is in 1 m/s. Those for 5, 7, and 10 m/s are thickened.

The variability is also low over tropical and subtropical oceans, as shown in Figure 3. The variability is higher in the storm tracks of North Pacific, North Atlantic, and the Roaring Fifties (over the circumpolar currents around Antarctica). The winds in these regions are strongest in their respective winter season. Much of the increase in root-mean-square deviations is due to these higher seasonal changes in high latitudes. High winds are usually transient and require high resolution (temporal and spatial).

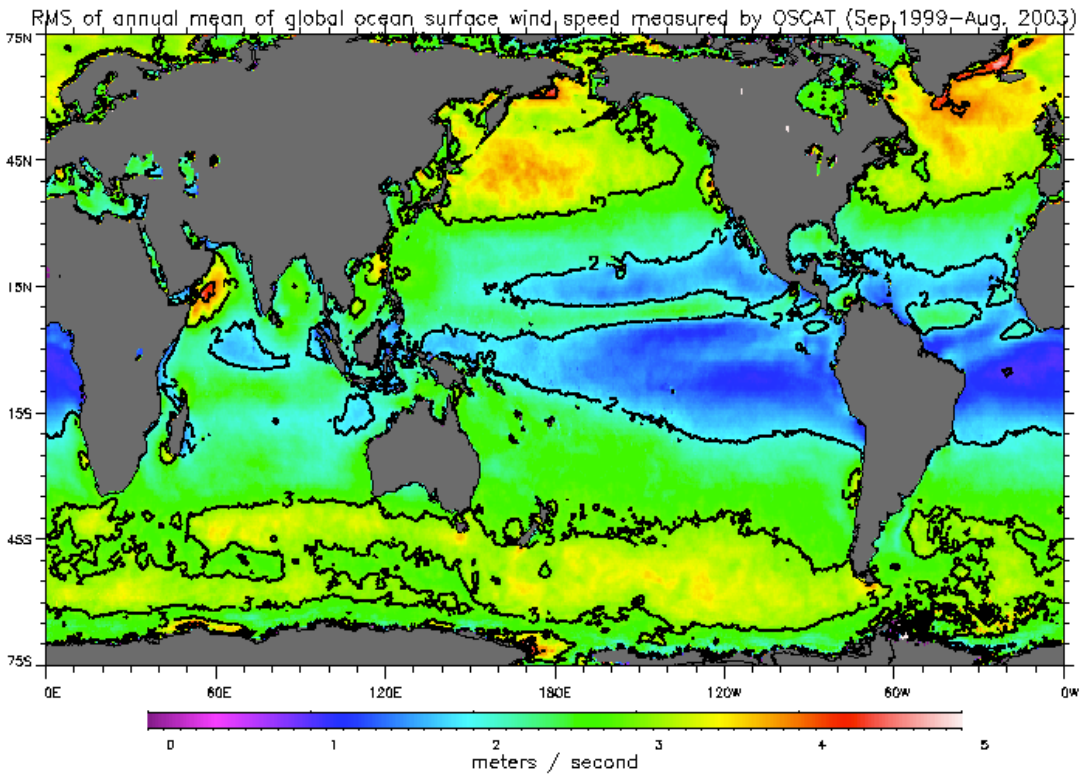

Figure 3. Root-mean-square deviation from the 4-year mean derived from daily winds from QuikSCAT. Isotachs are in m/s.

Section 3. Global Ocean Response

3.1 Wind Forcing

The wind data used in the oceanographic studies (described in Sections 3.2, 3.3, and 4) are obtained from the monthly averages of NCEP reanalysis fields for 2000. The direction error is modeled to be random and to have a white spectrum. The size of the error is at the maximum of ± 45° of the NCEP wind direction. Only if the wind speed is less than 7 m/s is the random error introduced. The introduction of directional wind error was performed to the 12-hourly wind field instead of time mean.

3.2 Ekman and Svedrup Transports

Ekman transport, which is the poleward transport of water near the ocean surface driven by winds, and Sverdrup transport, which is the poleward transport integrated over the ocean depth caused by wind-driven ocean circulation, are functions of a surface wind vector. They are computed from the wind fields described in Section 3.1. The Ekman transport is computed at 5° intervals from 10° to 45° in both hemispheres. Between 10°S and 10° N, the Coriolis force approaches zero, resulting in the singularity. The random direction error perturbs the Ekman transport by about 5% (Figure 4) at 10° N and 10° S. The perturbation is largest at 10° in both hemispheres and becomes smaller towards the higher latitudes. This latitudinal dependence arises because the wind stress tends to be greater in the subtropics than in the tropics. The size of the perturbation in the Ekman transport is very close to that in the zonal wind stress, since the relationship between the Ekman transport and the wind stress is linear.

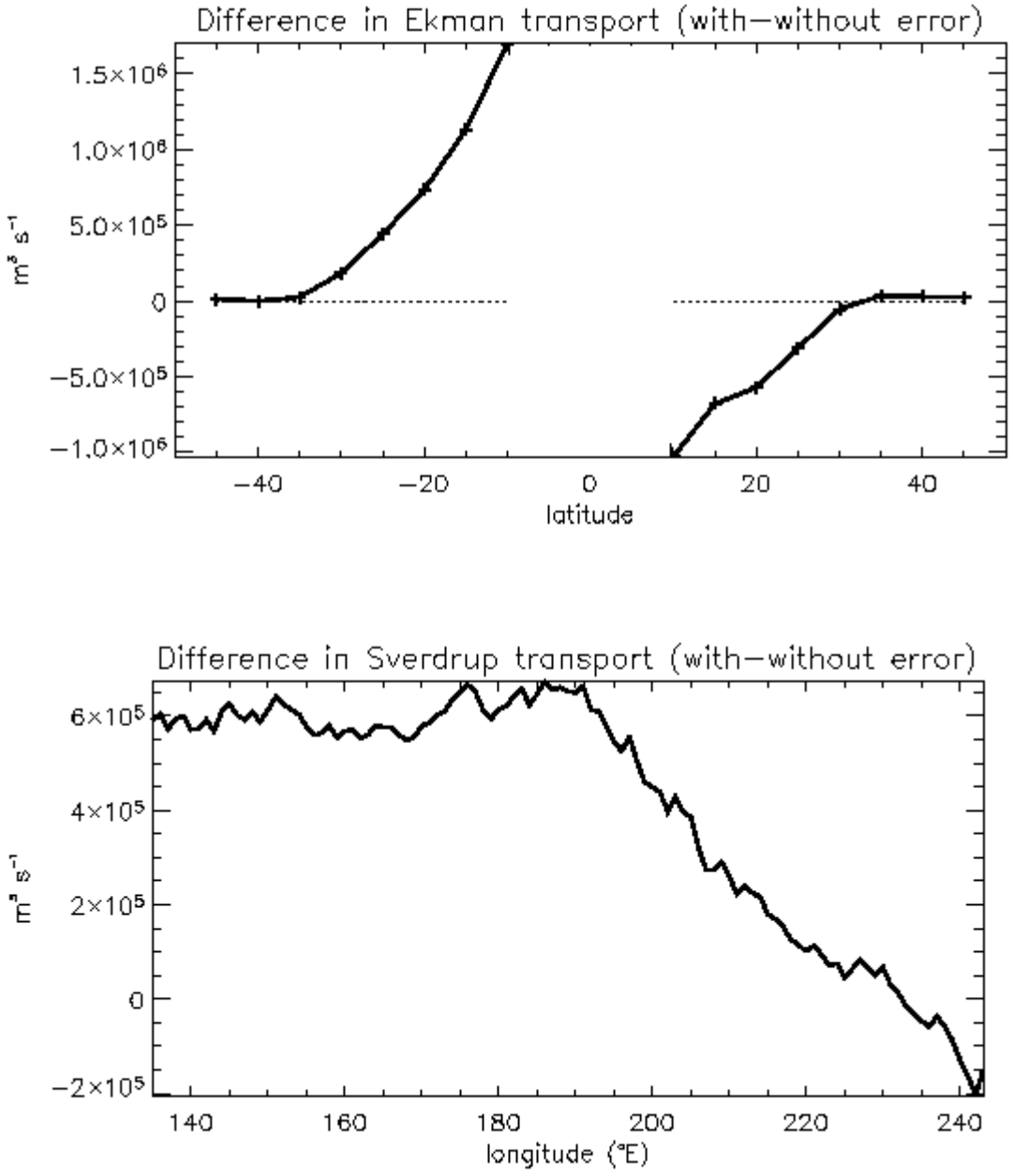

Figure 4. Impact of random directional wind error on time-mean zonally-integrated Ekman transport (upper) and Sverdrup transport across 30° N in the Pacific (lower).

It is interesting to observe that the absolute magnitude of the Ekman transport always decreases due to the random direction wind error. The reason is that the wind direction is predominantly zonal in the tropics where most of the perturbation occurs; therefore, the error acts to reduce the zonal wind speed even if the direction error is random.

The Sverdrup transport is computed by integrating the transport at one point, between the eastern and western boundaries of the oceans. In the subtropical gyre (between about 15° and 45° in latitude in both hemispheres), the directional error reduces the strength of the wind-driven gyre because of the weakening westerlies at around 45° and easterlies at around 15°. This reduction appears as positive and negative anomalies in the Northern and Southern Hemispheres respectively (Figure 5). The error in the zonal wind stress is more positive near 5° N than at 15° N due to more frequent perturbation at lower latitudes (Figure 7). This results in the positive perturbation in Sverdrup transport between 5° N and 15° N.

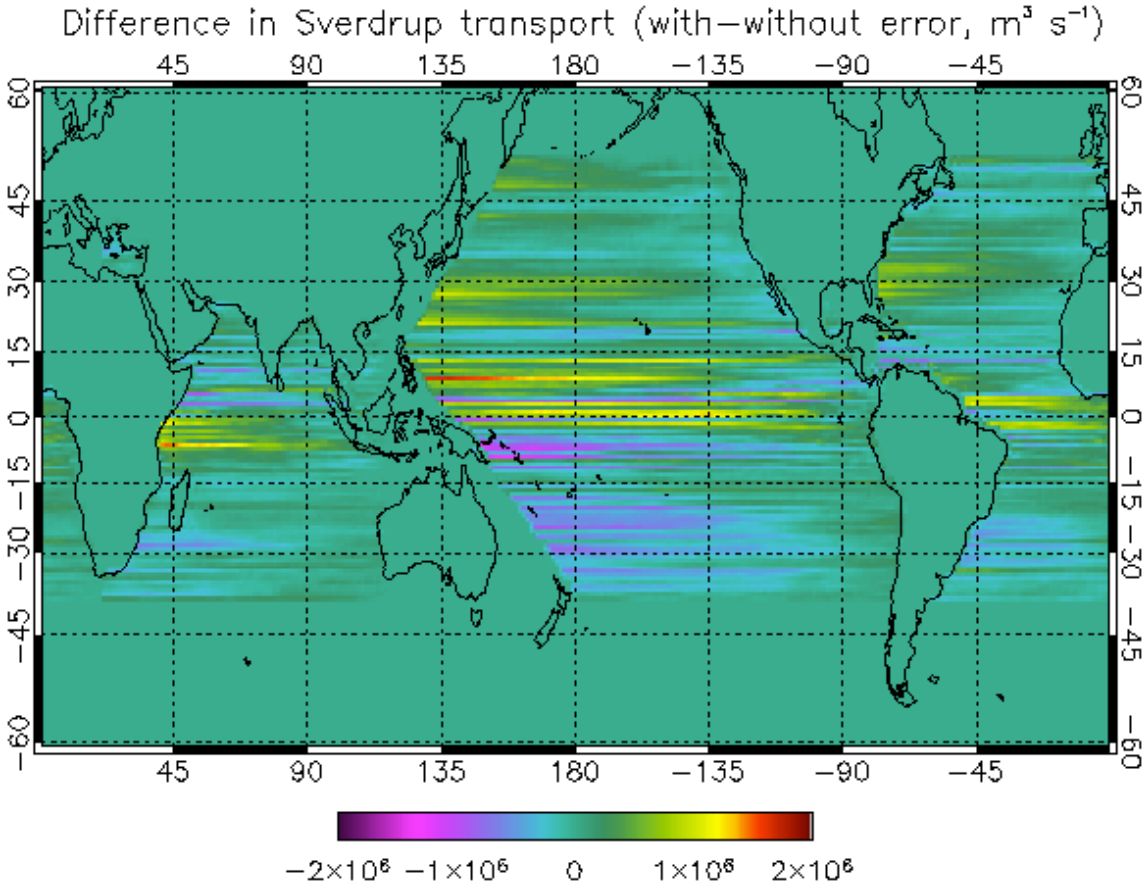

Figure 5. Impact of random directional wind error on time-mean zonally-integrated Sverdrup transport.

Around 30°N, where the wind stress curl is at maximum and therefore the wind-driven circulation is best represented (Sekine and Kutsuwada, 1994), the perturbation in the Sverdrup transport to the direction error is 3% (Figure 6). In the tropical Pacific, the Sverdrup transport varies by about 7% responding to the random error in the wind direction. The greater sensitivity in the tropics can be explained by the lower wind speed in the tropics than at 30°N, resulting in more frequent perturbation.

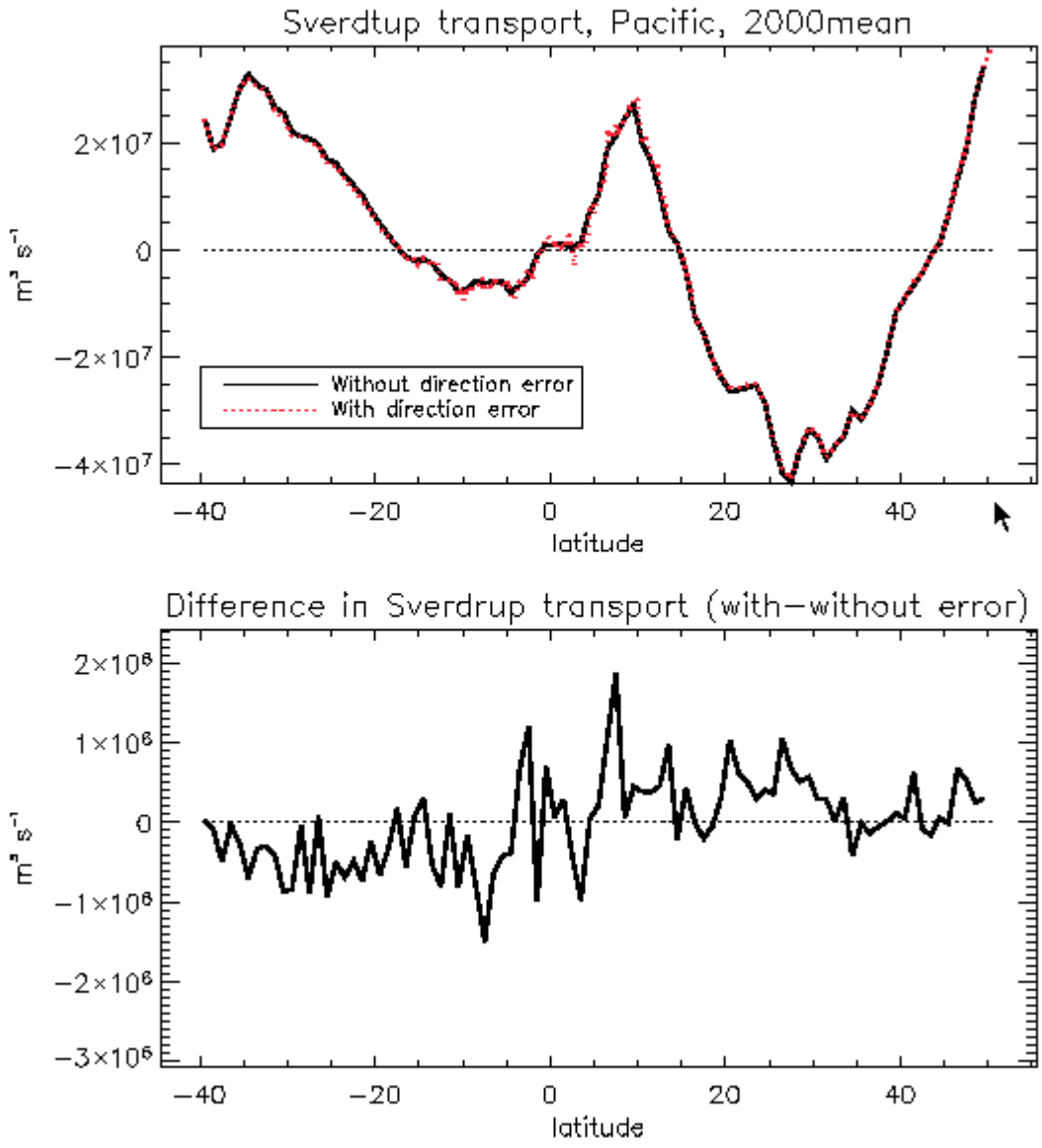

Figure 6. Impact of random directional wind error on time-mean zonally-integrated Sverdrup transport at various latitudes for the Pacific Ocean.

3.3 Simulation of Ocean's Response by OGCM

A global OCGM is used to evaluate the impact of random errors in the direction of weak wind (< 7 m/s). The model is the same as that used by Lee et al. (2002) to study the impact of the Indonesian throughflow on ocean circulation. Briefly, it is a version of the MIT OGCM (Marshall et al. 1997a) with a horizontal resolution of $1^o \times 0.3^o$ in the tropics and $1^o \times 1^o$ in the extratropics. There are 46 vertical levels with a depth increment ranging from 10 m above 150 m to intervals of 400 m at depth. Two advanced mixing schemes are employed: the so-called K-Profile Parameterization (KPP) vertical mixing (Large et al., 1994) and the GM isopycnal mixing (Gent and McWilliams, 1990). The model is forced at the surface by 12-hourly wind stress and by daily heat and freshwater fluxes obtained from the NCEP reanalysis (Kalnay et al., 1996).

The control and pertubation experiment are both one-year integrations (year 2000) forced by winds described in Section 3.1, with and without random directional errors. Figure 7 shows the difference in zonal wind stress with and without introducing the random directional error (upper panel). The random directional noises result in a westerly bias in the time-mean zonal wind in the tropical Pacific and Atlantic Ocean. This is because the wind over these regions is predominantly weak easterly wind. Therefore, any error in direction would cause a reduction of the easterly (i.e., introducing a westerly bias). The fact that a mid-latitude westerly has little bias is because wind is generally strong there and so little directional error perturbation is applied.

The lower panel of Figure 7 shows the impact of the directional wind error at sea level. The biased westerly in the perturbed wind causes the sea level to pile up in the eastern equatorial Pacific and Atlantic. The opposite is true for the equatorial Indian Ocean because the perturbed wind is more easterly (the mean wind is westerly there). Figure 8 shows the impact of the directional wind error on simulated temperature at sea surface and the near tropical thermocline (150 m). A bias of about 1^o C is seen in the eastern equatorial Pacific cold tongue region because the biased wind (more westerly) suppresses upwelling there by depressing the thermocline. The opposite is true off the western equatorial Pacific because thermocline is being lifted up. The 1^o C bias in the cold tongue region is quite substantial because it is as large as the threshold of anomalous temperature for that region that is used to define an El Niño.

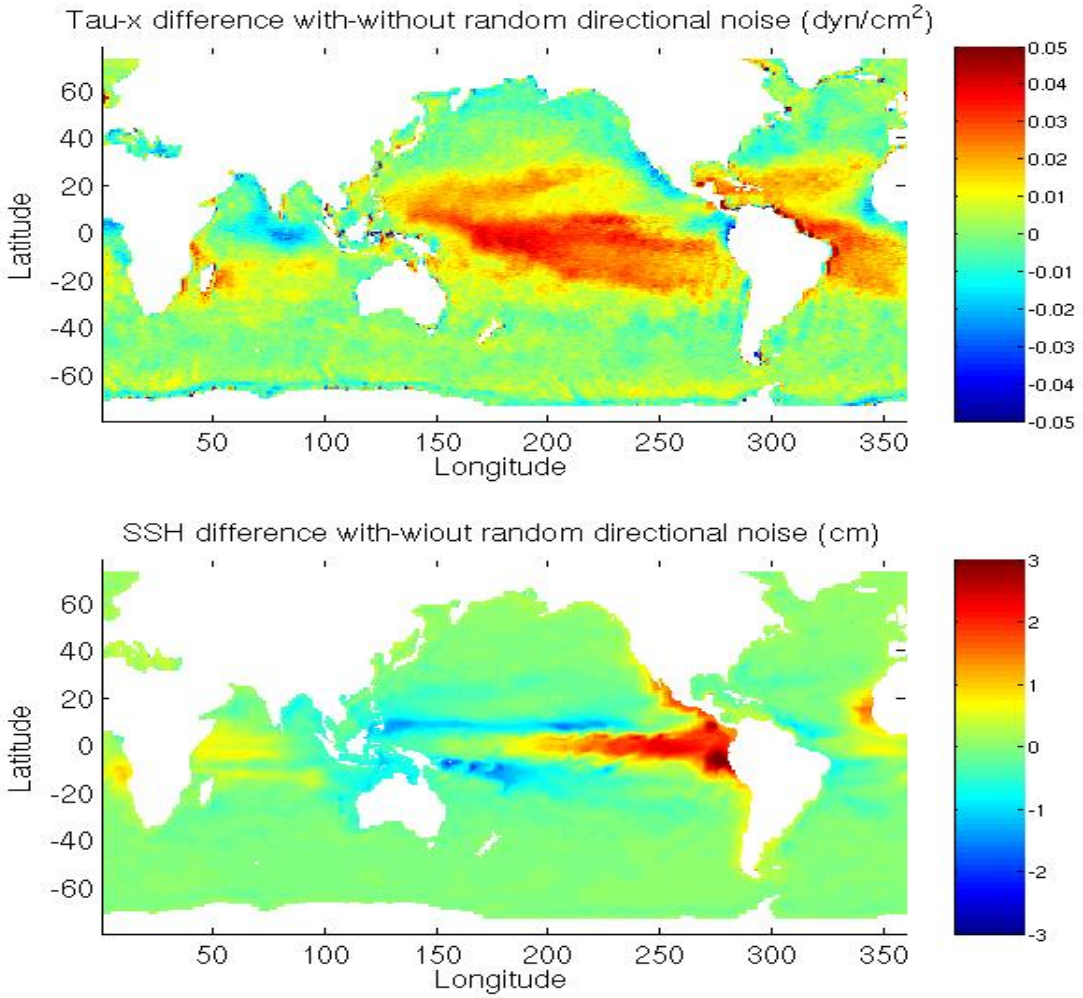

Figure 7. Impact of random directional wind error on time-mean zonal wind (upper) and sea level (lower).

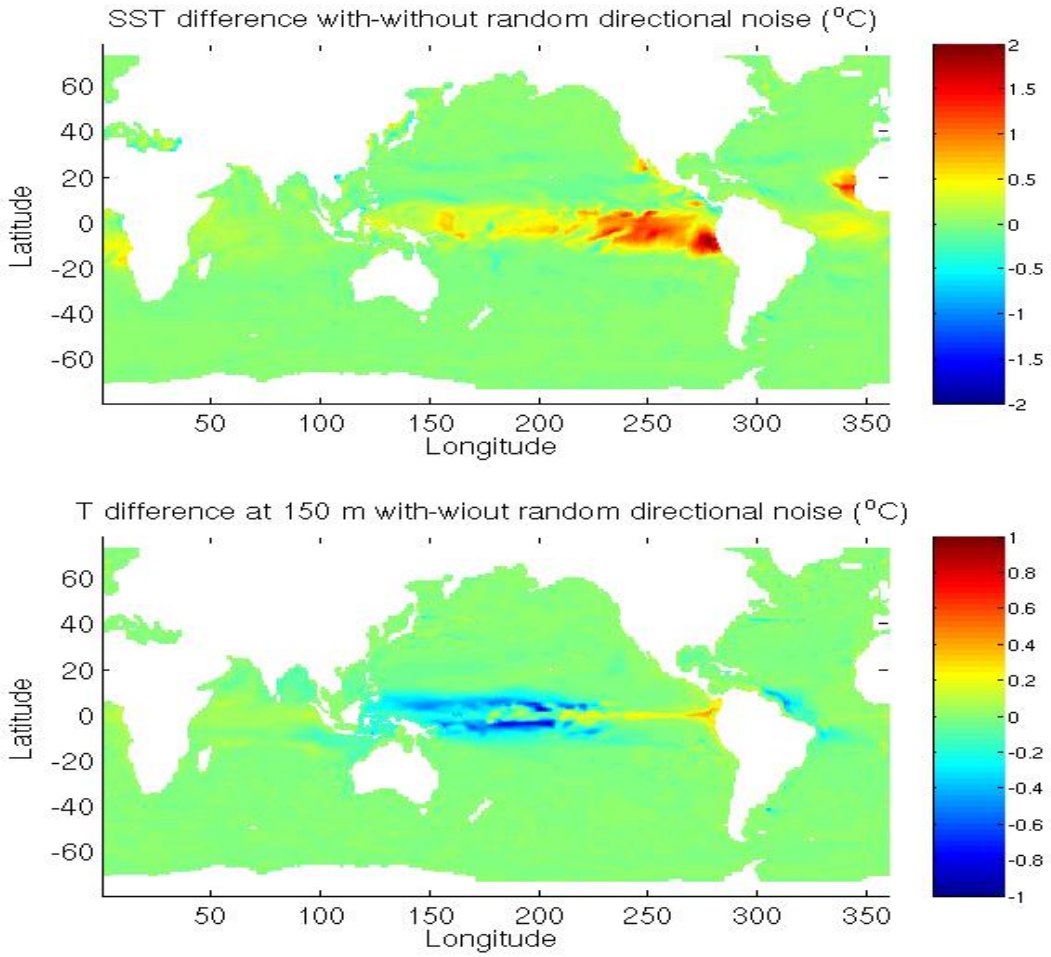

Figure 8. Impact of random directional wind error on time-mean temperature at sea surface (upper) and near tropical thermocline (150 m) (lower).

Figure 9 shows the impact on the meridional transport stream function (upper panel) and on meridional heat transport (lower panel), both integrated zonally around the globe. The meridional overturning circulation and poleward heat transport in the equatorial region are reduced by about 5% due to the random directional wind error.

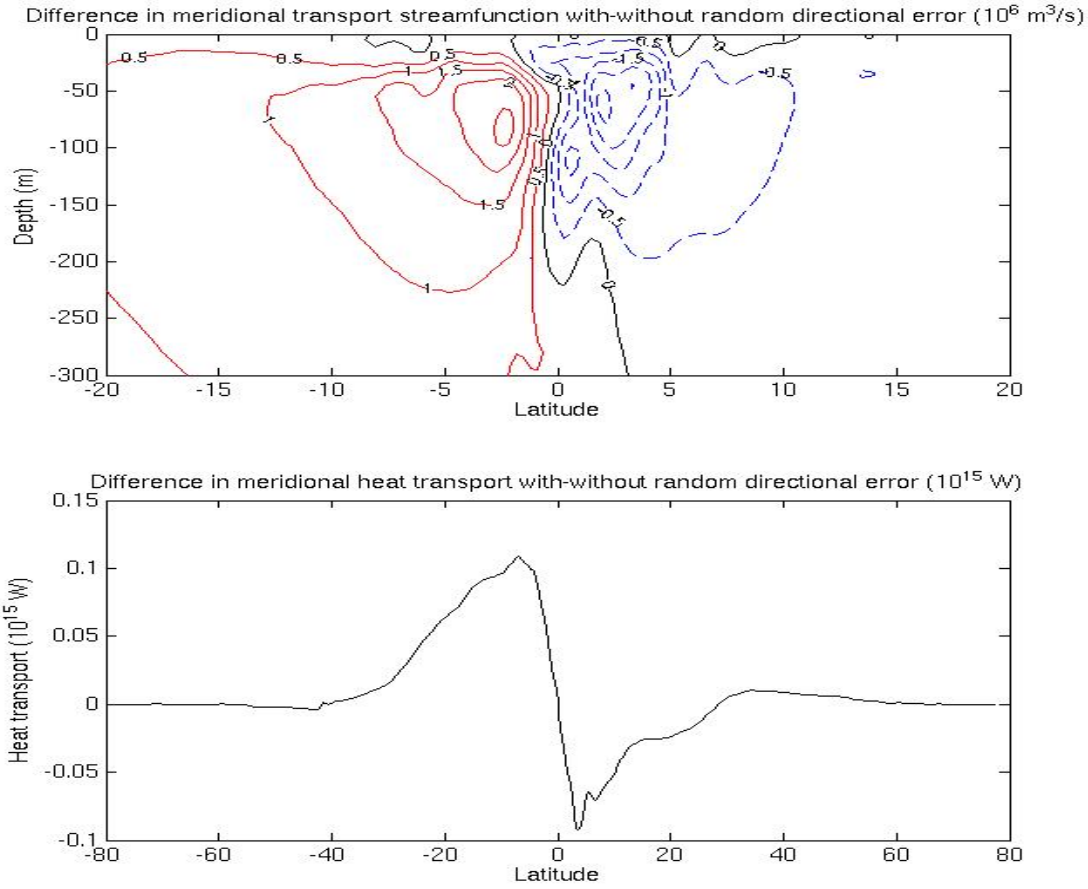

Figure 9. Impact of random directional wind error on time-mean meridional transport streamfunction (upper) and poleward heat transport (lower).

Section 4. Coastal Ocean Response

The coastal modeling experiments are based on the Regional Ocean Model System (ROMS), an evolution of the S-Coordinate Rutgers University Model (SCRUM), originally developed by Song & Haidvogel (1994). Similar to SCRUM, ROMS is a conservative, finite-volume discretization of the hydrostatic primitive equations in boundary-following coordinates with a variable free surface, Jacobian schemes for the pressure terms (Song, 1998), and includes new features of high-order upstream-biased advection, KPP mixing, and parallel computing capabilities (Shchepetkin & McWilliams, 2001). This model has been shown particularly suitable for coastal studies (e.g., Marchesiello et al., 2001).

Several other community ocean models are also available, including Modular Ocean Model (MOM) (Bryan, 1969), Miami Isopycnic-Coordinate Ocean Model (MICOM) (Bleck & Chassignet, 1994), Princeton Ocean Model (POM) (Blumberg & Mellor, 1987), and MIT model (Marshall et al., 1997b). Each of these models has its distinct advantages depending on specific applications. However, we have demonstrated expertise and experience with ROMS. In particular, several coastal and basin-scale models based on ROMS have been established on JPL's supercomputers. Based on these coastal and basin-scale models, we have developed a set of nested high-resolution coastal models for the United States West Coast in particular for this study.

Our basin-scale model is the Pacific Ocean with a horizontal resolution of a $0.5^{o} \times 0.5^{o}$ covering the area from 45° S to 65° N and 100° E to 70° W. The water depth is divided into 20 topography-following levels, with a minimum depth of 50 m near the coastal wall and a maximum depth of 5500 m in the deep ocean. The model starts with the initial conditions of annual mean temperature and salinity [Levitus et al., 1994]. The surface forcing are monthly mean air-sea fluxes of momentum, heat, and freshwater from NCEP/NCAR reanalysis. For the heat and salt flux, a thermal feedback term is applied. The model is first spun-up for 30 years with the annual-mean forcing, and then integrated from year 1948 to year 2003 by monthly-mean forcing. This basin-scale model provides open boundary conditions for our high-resolution United States West Coast model.

Our high-resolution United States West Coast model extends in latitude from 30^{o} N to 48^{o} N following the United States West Coastline. Using orthogonal curvilinear coordinates, the coastal region is divided into 480 × 520 grid cells, with an average grid size of 5 × 5 km. Such a fine-grid is necessary for resolving coastal features such as upwelling fronts, filaments, and eddies, as will be shown later. Although some of the coastal processes we will examine are internally driven and can be modeled regionally, most are driven by some combination of local and remote forcing. Therefore, the coastal model is nested into the Pacific Ocean model to offer a compromise for obtaining high-resolution in the coastal regions of interest and minimizing the overall computational coast, without losing the influence of the large-scale dynamics. The coastal model is run for 10 years (1991–2000) to reach a quasi-equilibrium state.

Our study focuses on the most representative coastal phenomena—wind-driven upwelling in the United States West Coast, which has characteristics of being remotely forced and locally intense. To assess the impact of the spatial and temporal variability of low winds on coastal circulations and upwelling fronts, we carried out two experiments. From the quasi-equilibrium solution (the 10th year), the coastal model continues for another run with the winds described in Section 3.1, and with the control runs and perturbation runs using winds, with and without adding directional errors.

Figure 10 shows the results from these two runs and their differences. The upper panel is the sea-surface height and the lower panel is the sea-surface temperature. Both results are 5-day averaged in July 10, 2001. Obvious differences can be seen between these two results, particularly in the SSH results that are directly related to wind stress curl. Although the perturbation run does not alter the large-scale pattern of the coastal water off the U. S. west coast, the difference is significant. The physical reason for this difference is that coastal upwelling is an unstable system and controlled by the balance between wind stress curl and cross-shelf pressure gradient force. Once the wind error is introduced, the balance has to be re-adjusted. Such an adjustment process can lead to baroclinic instability and result in different upwelling frontal patterns, eddy fields, and filaments. These are the results seen in the differences between these two runs.

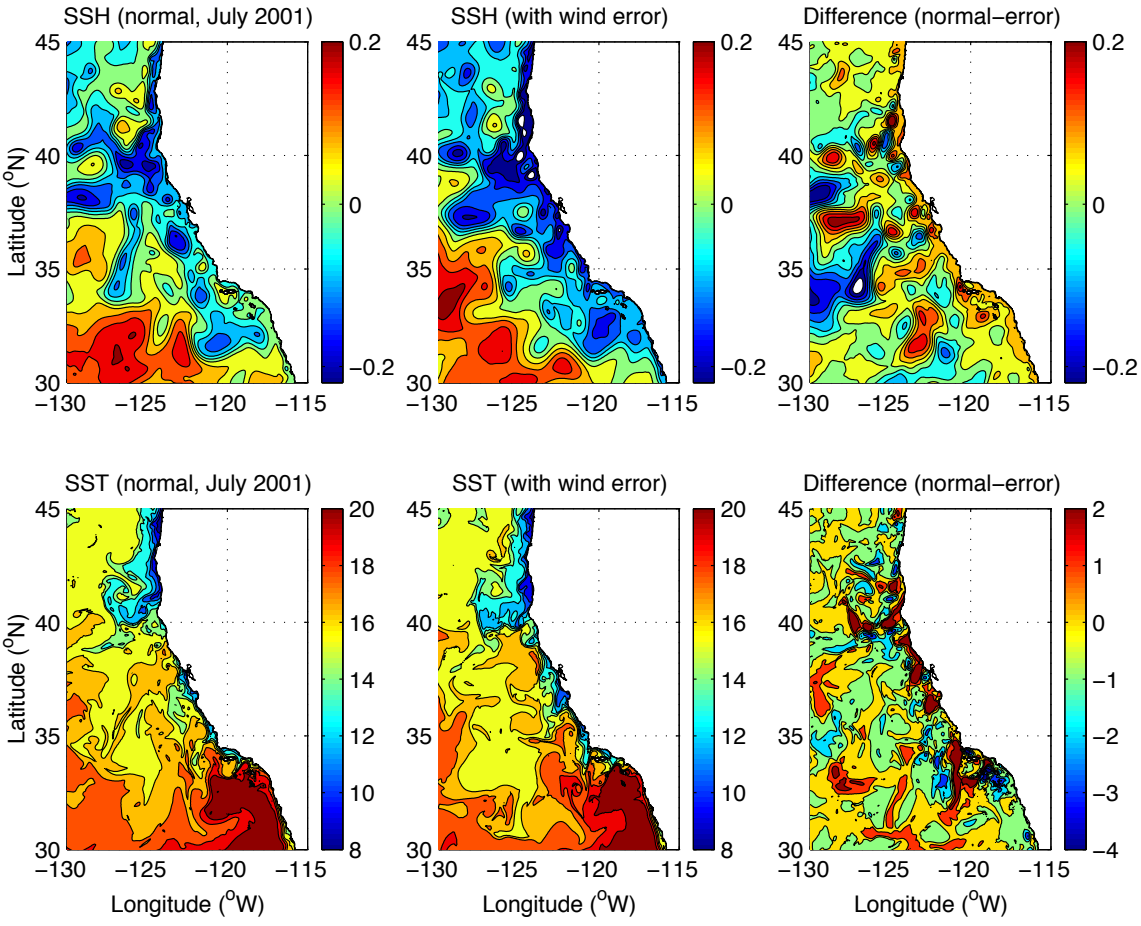

Figure 10. Model results from the two runs and their differences. The upper panel is the sea-surface height, and the lower panel is the sea-surface temperature. Both results are 5-day averaged centered in July 10, 2001.

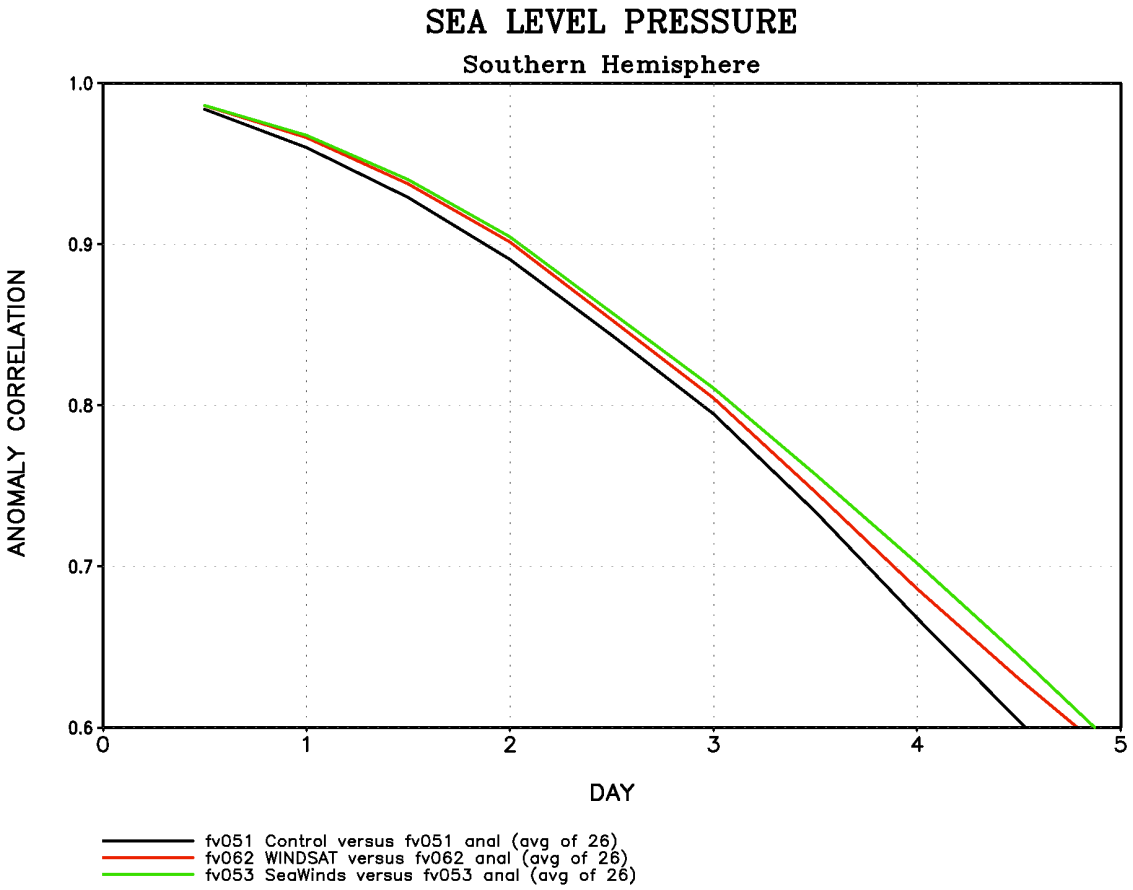

Figure 11. Forecast skill in Southern Hemisphere; black-control; green-SeaWinds, and red-perturbation.

Section 5. Numerical Weather Prediction

The Geosynchronous Earth Orbit Satellite (GEOS-4) data assimilation system, which is operational at NASA/GSFC was used to estimate the impact of directional errors on numerical weather prediction. GEOS-4 consists of the fvGCM (Finite Volume General Circulation Model) and PSAS (Physical Space statistical Analysis System). For the experiments described below, data assimilation was performed for the period of April 10, 2003 – May 15, 2003. The data assimilation experiments were each followed by a series of 26 five-day forecasts, starting on April 15 and running every day. Three experiments were conducted:

- "Control" run (includes no satellite surface winds used, but the full complement of operationally-used observational data);
- "SeaWinds" experiment (includes adds surface vector winds from SeaWinds on QuikSCAT to the "control");
- "Perturbation" run (includes "control" and SeaWinds data but with direction information removed from winds at or under 7 m/s).

In the PSAS analysis wind vectors above the surface layer of the atmosphere are used in a three-dimensional multivariate (wind/mass) analysis scheme. These wind vectors are computed from the scatterometer surface wind observations according to Monin-Obukhov similarity theory. Other (ship and buoy) surface wind observations are used the same way.

The results of the three experiments are shown in Figure 11. Anomaly correlation results represent the average of the 26 forecasts for each of the experiments. Anomaly correlation is an important measure of a forecast performance. It represents the correlation between forecast and observed departures from a mean climate state, and is a sensitive measure of differences in the pattern between forecast and observed fields. The green curve ("SeaWinds") shows that adding scatterometer winds improves both the skill and the prediction period over the black curve ("control"), while the red curve ("perturbation") shows that part of this improvement is lost when the directional information for wind speed under threshold is removed. The impact loss varies from 41% – 46% for 3–4 day forecasts.

Section 6. Discussion

We used constructed winds to illuminate the significance of accurate wind direction measurements under weak wind conditions. The percentage change in the anomaly correction in NWP, the Ekman and Sverdrup transports are, as expected, small because they are integrated over global oceans or across ocean basins. Yet, their impact on our characterizing and understanding of weather and climate changes may still be very significant. The strong impact in tropical oceans where the trade wind dominates is clearly evident. The impact on NWP is significant in the 3–4 day forecast range.

REFERENCES

Bleck, R. and E. P. Chassignet, 1994: "Simulating the oceanic circulation with isopycnic-coordinate models," *The Oceans*, Majmdar et al. (eds.), The Pennsylvania Academy of Science, pp. 17-39.

Blumberg, A. F., and G. L. Mellor, 1987: "A description of a three-dimensional coastal ocean circulation model," *Vol. 4, Three-Dimensional Coastal Ocean Models*. N. Heaps (ed.), AGU, 208 pp.

Freilich, M. and R.S. Dunbar, 1999: "The accuracy of the NSCAT 1 vector winds: comparisons with National Data Buoy center buoys," *J. Geophys. Res.*, **104(C3),** 11,231–11,246,.

Gent, P. and J. McWilliams, 1990: "Isopycnal mixing in ocean circulation models," *J. Phys. Oceanogr.*, **20**, 150–155.

Kalnay, E., M. Kanamitsu, R. Kistler, et al., 1996: "The NCEP/NCAR 40-year reanalysis project," *Bull. Amer. Meteorol. Soc.*, **77**, 437–471.

Large, W.G., J.C. McWilliams, S.C. Doney, 1994: "Oceanic vertical mixing: a review and a model with a non local boundary layer parameterization," *Rev. Geophys.*, 363–403.

Lee, T., I. Fukumori, D. Menemenlis, Z. Xing, and L.-L. Fu, 2002: "Effects of the Indonesian throughflow on the Pacific and Indian Oceans," *J. Phys. Oceanogr.*, **32**, 1404–1429.

Levitus, S., R. Burget, and T. Boyer, 1994: "World Ocean Altas: Salinity and Temperature 3–4," *NOAA Altas NESDID, U. S. Dept. Commerce*.

Marchesiello, P., J. C. McWilliams, and A. Shchepetkin, 2003: "Equilibrium structure and dynamics of the California current system," *J. Phys. Oceanogr.* **33**. 753-783.

Marshall, J., A. Adcroft, C. Hill, L. Perelman, and C. Heisey, 1997a: "A finite-volume, incompressible Navier-Stokes model for studies of the ocean on parallel computers," *J. Geophys. Res.*, **102**, 5753–5766.

Marshall, J., C. Hill, L. Perelman, and A. Adcroft, 1997b: "Hydrostatic, quasi-hydrostatic and non-hydrostatic ocean modeling," *J. Geophys. Res.*, **102**, 5733–5752.

Plant, W.J., 2000: "Effects of wind variability on scatterometry at low wind speeds," *J. Geophys. Res.*, **10**5, 16,899–16,910.

Roemmich, D. and C. Wunsch, 1985: "Two transatlantic sections: meridional circulation and heat flux in the subtropical North Atlantic Ocean," *Deep Sea Res.*, **32**, 619–664.

Sekine, Y. and K. Kutsuwada, 1994: "Seasonal variation in volumen transport of the Kuroshio south of Japan," *J. Phys. Oceanogr.*, **24,** 261–272.

Shchepetkin, A. F., and J. C. McWilliams, 2001: "The regional ocean modeling system: a split-explicit, free-surface, topography-following coordinate ocean model," *UCLA*, 31pp.

Song, Y. T., and D. B. Haidvogel, 1994: "A semi-implicit ocean circulation model using a generalized topography-following coordinate," *J. Comput. Phys.*, **115**, 228–244.

Song, Y. T., 1998: "A general pressure gradient formulation for ocean models. Part I: Scheme design and diagnostic analysis," *Mon. Wea. Rev,.* **126**, 3212–3230.

Yueh, S.H., W.J. Wilson, S.J. Dinardo, F.K.Li, 1999: "Polarimetric microwave brightness signatures of ocean wind directions," *IEEE Trans. Geosci. Remote Sensing*, **37(2),** 949–959.